Applied and Environmental Microbiology, Dec. 2008, p. 7410–7421 Vol. 74, No. 23
0099-2240/08/$08.00+0 doi:10.1128/AEM.01710-08

Comparative Characterization of the Microbial Diversities of an Artificial Microbialite Model and a Natural Stromatolite▽†

Stephanie A. Havemann and Jamie S. Foster*

Department of Microbiology and Cell Science, University of Florida, Space Life Sciences Laboratory, Kennedy Space Center, Florida 32899

Received 24 July 2008/Accepted 25 September 2008

Microbialites are organosedimentary structures that result from the trapping, binding, and lithification of sediments by microbial mat communities. In this study we developed a model artificial microbialite system derived from natural stromatolites, a type of microbialite, collected from Exuma Sound, Bahamas. We demonstrated that the morphology of the artificial microbialite was consistent with that of the natural system in that there was a multilayer community with a pronounced biofilm on the surface, a concentrated layer of filamentous cyanobacteria in the top 5 mm, and a lithified layer of fused oolitic sand grains in the subsurface. The fused grain layer was comprised predominantly of the calcium carbonate polymorph aragonite, which corresponded to the composition of the Bahamian stromatolites. The microbial diversity of the artificial microbialites and that of natural stromatolites were also compared using automated ribosomal intergenic spacer analysis (ARISA) and 16S rRNA gene sequencing. The ARISA profiling indicated that the Shannon indices of the two communities were comparable and that the overall diversity was not significantly lower in the artificial microbialite model. Bacterial clone libraries generated from each of the three artificial microbialite layers and natural stromatolites indicated that the cyanobacterial and crust layers most closely resembled the ecotypes detected in the natural stromatolites and were dominated by *Proteobacteria* and *Cyanobacteria*. We propose that such model artificial microbialites can serve as experimental analogues for natural stromatolites.

Microbialites are complex microbial mat ecosystems that have a propensity for trapping, binding, and precipitating organosedimentary structures (11). Although there are numerous examples of naturally occurring microbial mat communities that trap and bind sediments (15, 20), few ecosystems are conducive to the processes of lithification and fossilization (20, 52). The microbial mats that do undergo lithification produce a variety of carbonate precipitates, the structures of which are dependent on the microbial community composition, the predominant metabolic pathways, and the surrounding geochemical conditions (3, 21).

Microbialites are categorized by the extent of layering within the community (20). Those microbialites with well-laminated, lithified structures are known as stromatolites (31). Fossil evidence suggests that for over 3 billion years stromatolites were ubiquitous on Earth (5, 29); however, modern analogues of these ancient communities are found today only in a few remote locations around the globe (29). One such site is the island of Highborne Cay, which is located along the west margins of Exuma Sound, Bahamas. The stromatolites of Exuma Sound represent the only known example of actively accreting stromatolites in normal marine salinity (17, 18, 48).

The stromatolites of Highborne Cay are composed primarily of oolitic sand grains trapped and embedded in a biogenic matrix of exopolymeric substances (EPS) (Fig. 1A). Over time, biologically induced lithification of the oolitic sand grains results in periodic deposition of calcium carbonate, primarily as aragonite (98%) (49, 58). The calcium carbonate deposition occurs in conjunction with boring of sand grains by endolithic microbes (39, 44), resulting in cementation of the sand grains, which ultimately form horizontal laminae throughout the microbialite subsurface (Fig. 1B) (49). A stromatolite at Highborne Cay grows by continual accretion of the biogenic EPS layer and trapping and binding of new sand grains (45). The microbial mat associated with stromatolite accretion is dominated by filamentous and coccoid cyanobacteria, which comprise a conspicuous phototrophic layer in the top 5 mm of the community (Fig. 1B) (27, 49). These oxygenic phototrophs are the dominant primary producers in the stromatolite ecosystem, driving the fixation of carbon dioxide into organic substrates (40, 41, 59).

Morphological and biogeochemical analyses of the Highborne Cay communities have revealed several other key microbial functional groups associated with the stromatolites, including aerobic heterotrophs, sulfide-oxidizing bacteria, sulfate-reducing bacteria, and fermentative bacteria (56–58). Biochemical signatures of these metabolisms have been found in close association with the cyanobacterial layer in stromatolites (59). Together, these microbes generate distinctive light-driven geochemical gradients that vary throughout the diel cycle (49).

All of the previous studies of the biocomplexity and biogeochemistry of microbial mats have relied on in situ measurements or on transferring mature communities to the laboratory environment. Stochastic, in silico models have provided insight into the role of microbial mat composition and environmental conditions in stromatolite morphology and growth (19); however, these computer-based models have not been comple-

* Corresponding author. Mailing address: Department of Microbiology and Cell Science, University of Florida, Space Life Sciences Laboratory, Kennedy Space Center, FL 32899. Phone: (321) 861-2900. Fax: (321) 861-2925. E-mail: jfoster@ufl.edu.

† Supplemental material for this article may be found at http://aem.asm.org/.

▽ Published ahead of print on 3 October 2008.

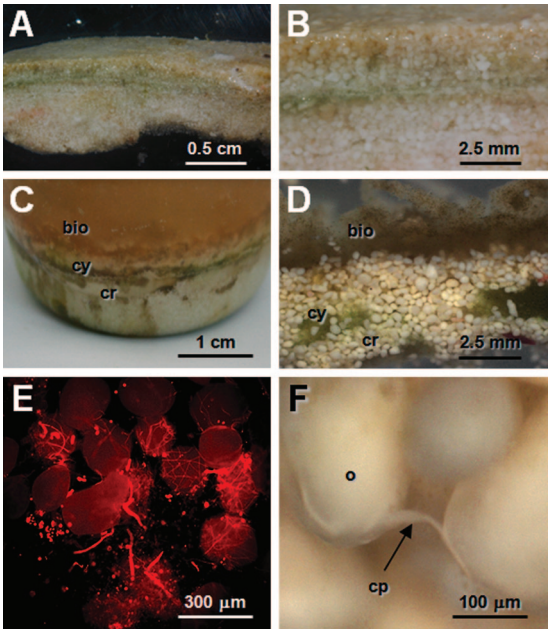

FIG. 1. Morphological overview of natural stromatolites and artificial microbialites. (A) Section of a field-collected natural stromatolite from Highborne Cay, Bahamas. (B) Cross section of a natural stromatolite. (C) Side view of an artificial microbialite grown under laboratory conditions, showing the three primary layers, the biofilm layer (bio), the cyanobacterial layer (cy), and the crust layer (cr). (D) Cross section of an artificial, laboratory-cultivated microbialite. (E) Autofluorescence of a sample taken from the cyanobacterial layer, indicating extensive diversity and colonization by cyanobacteria. (F) Light micrograph of ooids (o) taken from the crust layer, showing extracellular calcium carbonate precipitation (cp).

mented yet with experimentally manipulable in vitro models. There are numerous examples of cultivated cyanobacterial microbial mats from Antarctic lakes (10), hypersaline ecosystems (1, 7, 28), and marine ecosystems (22–24); however, only a single laboratory cultivated mat has been shown to undergo lithification in vitro (25). In this mat system, carbonate deposition was not laminated and was examined using only microscopy (25). Although this previous study carefully elucidated the general zonation of the major functional groups with the artificial mats, it did not provide a molecular analysis of the microbial diversity associated with the mat or site of carbonate deposition.

In this study, we demonstrated that stromatolitic microbialite formation can be initiated under laboratory conditions, generating layered microbial communities that are morphologically and functionally similar to the natural lithifying communities. We propose that artificial microbialites can ultimately serve as experimental model systems for the development of nascent stromatolite communities, thus elucidating biogenic factors associated with the initiation of these dynamic microbial ecosystems.

MATERIALS AND METHODS

Sampling of natural stromatolites. Stromatolites were collected in July 2006 from the intertidal zone of Highborne Cay, Bahamas. Sections of type 2 stromatolites (i.e., carbonate-depositing microbial mats with a superficial micritic crust) were excised (50 g) in triplicate from site 8 and stored in separate plastic containers containing natural seawater. Detailed descriptions of stromatolite type and site designations have been given previously (49). The samples were transported at room temperature to the Space Life Sciences Laboratory (Kennedy Space Center, FL), where they were maintained in artificial seawater aquaria until further processing. Additional core samples were taken from the same stromatolites with a Harris Uni-Core (8 mm; Ted Pella, Redding, CA) and stored at −80°C in 1.5-ml microcentrifuge tubes containing 500 μl of RNA*later* (Ambion, Austin, TX). Oolitic sand grains were also collected from site 8 and stored in 1-gallon Ziploc bags until they were sterilized.

Artificial microbialite initiation and growth. Three stromatolite sections (50 g) were homogenized and added to plastic dishes that contained sterilized ooids to a depth of approximately 1 cm. The inoculated ooids were placed into 10-gallon aquaria containing 1× artificial seawater (Instant Ocean, Mentor, OH) and were maintained at 30°C with 35‰ salinity, 400 ppm carbon dioxide, and 300 microeinsteins/m^2/s of light using a cycle consisting of 12 h of light and 12 h of darkness for 1.5 years. The tanks were aerated using a Whisper Air Pump 10 (Tetra, Blacksburg, VA) and sterilized airstones. Microscopy was performed using an Olympus (Center Valley, PA) SZX12 zoom stereo microscope and a Carl Zeiss (Jena, Germany) Axioskope 40.

To examine the specific polymorph of calcium carbonate in the artificial microbialites, X-ray diffraction (XRD) was used. After 1.5 years of growth and development, carbonate precipitates were dissected from artificial microbialites and natural stromatolites, dried, and ground with a sterile mortar and pestle. The ground carbonates were analyzed with a Philips APD 3720 powder XRD in Bragg-Brentano geometry at 2°Theta.

Extraction of DNA from artificial microbialites and natural stromatolites. The artificial microbialites were separated on the basis of three distinct layer types, the upper biofilm layer (thickness range, 2 to 5 mm), the middle cyanobacterial layer (range, 0.5 to 2 mm), and the bottom crust layer (range, 0.5 to 1 cm). Ten slices of each layer weighing 75 to 85 mg each were then added to individual 2-ml cryotubes containing a sterile zirconia bead cocktail (0.2 g of 0.1-mm beads, 0.2 g of 0.7-mm beads, and 0.2 g of 2.4-mm beads; BioSpec Products, Inc., Bartlesville, OK). Natural stromatolite core samples were thawed to room temperature and washed three times in sterile water. Ten vertical slices weighing 75 to 85 mg each were added to individual 2-ml cryovials containing the bead cocktail mentioned above. These samples were stored overnight at −20°C to assist in lysis of the cells. Total genomic DNA was extracted from the samples using a modified xanthogenate DNA extraction procedure (28, 55). DNA concentrations were determined spectrophotometrically (NanoDrop 1000; Thermo Fisher Scientific, Wilmington, DE).

ARISA. Due to the heterogeneity of the intergenic transcribed spacer (ITS) region in prokaryotes, the automated rRNA intergenic spacer analysis (ARISA) method enables rapid assessment of the microbial diversity within a targeted community (26, 36, 62). Universal bacterial ARISA was performed for all samples using the general S-D-Bact-1522-b-S-20 and L-D-Bact-132-a-A-18 primers, which amplify the region between position 1452 of the 16S rRNA gene and position 115 of the 23S rRNA gene of *Escherichia coli* (13, 47). The 25-μl PCR mixtures contained (final concentrations) 1× GoTaq colorless reaction buffer (Promega, Madison, WI), 1.5 mM $MgCl_2$, 160 μM deoxynucleoside triphosphates, 100 μg/ml bovine serum albumin, 400 nM of each primer, 15 ng of genomic DNA, 2.5 U GoTaq Flexi DNA polymerase (Promega), and water. Initially, the reaction mixtures were kept at 94°C for 3 min, and this was followed by 30 cycles of amplification at 94°C for 1 min, at 55°C for 30 s, and at 72°C for 1 min and a final extension at 72°C for 7 min.

Each reaction mixture was loaded into chip wells that were prepared according to the manufacturer's recommendations (DNA 1000 LabChip kit; Agilent Technologies, Santa Clara, CA). Samples were analyzed using an Agilent 2100 bioanalyzer and the Agilent 2100 Expert software program. The Agilent software determined peak sizes (in base pairs) and areas based on data for internal size standards in each lane (15 and 1,500 bp) and an external ladder. To include the maximum number of peaks while excluding background fluorescence, a threshold of 20 fluorescence units greater than the baseline was set manually. Peak sizes were compared for all 40 samples; the values within ±5% were assumed to be the same according to the kit instructions and were averaged to obtain the peak sizes reported here.

To recover specific peaks of interest, five identical PCRs for each target sample were performed as described above. Samples were pooled, and the product was ethanol precipitated. Products were resuspended in 40 μl of 1 mM Tris-HCl (pH 8.5) and 8 μl of 6× DNA loading dye (10 mM Tris-HCl [pH 7.5], 50 mM EDTA [pH 8.0], 0.03% bromophenol blue, 15% Ficoll 400). Samples were run on a 2.5% agarose gel, and bands that corresponded to peaks of interest were excised and purified using a Qiagen gel extraction kit according to the manufacturer's protocol (Qiagen, Valencia, CA). Samples were then cloned into

the vector pCR2.1 using an Original TA cloning kit according to the manufacturer's instructions (Invitrogen, Carlsbad, CA). At least five positive clones of each sample were selected and sequenced by the Sanger method with the T7 forward primer at the University of Florida Interdisciplinary Center for Biotechnology Research DNA Sequencing Core Facility.

Statistical analysis of ITS data and ITS clone libraries. Once the peak sizes and significance were determined, the peak areas were imported into the Primer 6 software package (version 6.1.10) and normalized using the $\log(X + 1)$ pretreatment function. Samples were then analyzed using the Bray-Curtis similarity method (8) and clustered in the complete linkage mode with the default parameters (5% significance; mean number of permutations, 1,000; number of simulations, 999) to generate a phylogenetic tree based on percent similarity. A multidimensional scaling plot was then generated using the default parameters with a minimum stress of 0.01 to generate a configuration plot based on percent similarity.

Diversity indices were calculated from the nontreated peak areas to generate the Margalef species richness value, the Shannon index, and Pielou's evenness value for the 34 artificial and natural microbialite samples that generated significant bands. The values for the representatives of each of the four samples types were then averaged to generate the biofilm, cyanobacterial, crust, and natural stromatolite diversity indices. The overall artificial microbialite index was generated by averaging the values for all the biofilm, cyanobacterial, and crust samples. Sequences of the 16S-23S rRNA ITS region were analyzed to ascertain their closest relatives by using the basic local assignment and search tool (BLASTn) function of the GenBank database (National Center for Biotechnology Information) (2).

Generation and sequencing of 16S rRNA gene clone libraries. DNA from 10 replicates of the artificial microbialite layers and the natural stromatolites were independently pooled. The 16S rRNA gene of each of the four pooled samples (10 ng) was PCR amplified using universal bacterial primers 27f (AGAGTTTG ATCCTGGCTCAG) and 1525r (TAAGGAGGTGATCCAGCC) (35). The 25-μl PCR mixtures contained (final concentrations) 1× GoTaq colorless reaction buffer, 1.5 mM $MgCl_2$, 240 μM deoxynucleoside triphosphates, 100 μg/ml bovine serum albumin, 400 nM of each primer, 2 U GoTaq Flexi DNA polymerase, and water. Initially, the reaction mixtures were kept at 94°C for 5 min, and this was followed by 30 cycles of amplification at 94°C for 1 min, at 58°C for 1 min, and at 72°C for 2 min and a final extension at 72°C for 7 min. PCR products were cloned as described above, and 597 products were picked for sequencing.

Statistical analysis of 16S rRNA gene clone libraries. The partial 16S rRNA gene sequences obtained in this study were aligned with known bacterial sequences using the Greengenes 16S rRNA NAST alignment tool (16). The aligned sequences were then screened to identify chimeric sequences using the Bellerophon tool on the Greengenes website (30) and the Chimera Detection program at the Ribosomal Database Project website (14). Fifteen putative chimeric sequences were removed from the artificial microbialite and natural stromatolite clone libraries. The remaining 582 aligned 16S rRNA gene fragments were classified using the Greengenes Automatic Taxonomic Classification tool.

A distance matrix was also constructed based on the aligned forward sequences (5′-to-3′ direction from the start of the 16S rRNA gene) using the Greengenes Distance Matrix calculator. The distance matrix output of Greengenes was then used to generate rarefaction curves using the software package DOTUR (51). The percent coverage of the libraries was determined using the following equation: percent coverage $= [1 - (n/N)] \times 100$, where n is the number of single-coverage operational taxonomic units (OTUs) and N is the total number of sequences. All aligned 16S rRNA sequences ($n = 582$) were imported into the Greengenes sequence database using the ARB software package with the ARB parsimony option and a 50% maximum frequency bacterial filter (38).

Nucleotide sequence accession numbers. The ITS sequences have been deposited in the GenBank database under accession numbers EU917446 to EU917539, and the 16S rRNA sequences have been deposited in the GenBank database under accession numbers EU917540 to EU918121.

RESULTS

Cultivation and morphology of artificial microbialites. Inoculation of sterile oolitic sand grains with homogenized field-collected stromatolite material resulted in the formation of multilayer microbialite communities. Distinctive layers within the community were visible after 2 months. After 1.5 years of incubation in artificial light and seawater conditions, the microbialites had three pronounced layers (Fig. 1C and D). The uppermost layer of the microbialites consisted of a thick biofilm (range, 2 to 5 mm) of coccoid and rod-shaped bacteria attached to filamentous cyanobacterial sheaths encased in a matrix of EPS. In the absence of periodic burial with sterile ooids, the biofilm layer accreted until it was over 1 cm thick. Underneath the EPS-rich biofilm was a layer of cyanobacteria associated with a loose aggregation of ooids that did not form a calcium carbonate crust. The cyanobacterial layer (range, 0.5 to 2 mm in depth) consisted of three morphotypes: filamentous, coccoid, and pseudofilamentous morphotypes (Fig. 1E). The deepest layer of the cultivated microbialites, between 0.5 mm and 1 cm, was composed of a lithified crust layer of oolitic sand grains fused by extracellular calcium carbonate precipitation (Fig. 1F). The composition of calcium carbonates dissected from the artificial microbialite crust layer was compared to the composition of calcium carbonates found in natural stromatolites using XRD analyses. The XRD results suggested that the calcium carbonates in the artificial and natural communities were highly similar and comprised predominately of the polymorph aragonite (Fig. 2). Sterilized sand grains that were maintained axenically under similar artificial growth conditions did not form any lithified organosedimentary structures.

Community diversity profiles of artificial and natural microbialites using ARISA. The three layers of the artificial microbialites (biofilm, cyanobacterial, and crust layers) were compared to the layers of the intact natural stromatolites using ARISA. The layers of the natural stromatolites were not horizontally sectioned due to the extensive lithification of the microbial mat lamina. Amplification of the ITS region between the 16S and 23S rRNA genes generated 21 significant peaks for the four communities analyzed. The ARISA profiles of the samples, including the number of peaks, the peak size, and the peak area, are shown in Table 1. Overall, there was a 67% overlap in community ITS patterns between the combined artificial microbialites (i.e., the biofilm, cyanobacterial, and crust layers) and the natural stromatolites.

The ARISA profiles shown in Table 1 were used to generate a phylogenetic tree based on percent similarity, as calculated by the Bray-Curtis measure (Fig. 3A). The percent similarities for the ITS profiles of all four communities are shown in a multidimensional scaling plot in Fig. 3B. The highest level of similarity was the level of similarity between the artificial microbialite crust and cyanobacterial layers, in which 40 to 50% of the ITS profiles overlapped. The ARISA profiles of the natural stromatolites were clustered in two distinct populations; one group was more closely related to the cyanobacterial and crust layers (20 to 40%), and the other group was more closely related to the biofilm layer (20%). Higher levels of similarity were detected when individual samples were compared (Fig. 3B). For example, a subset of the crust sample (sample Cr4) shared 60% of the ITS banding profile between the natural stromatolite samples (samples S7 and S8). One biofilm sample (sample B5) was highly divergent, and its ARISA profile was less than 10% similar to the ARISA profiles of the other communities.

Diversity indices were also calculated from the ARISA profiles (Table 2). The species diversity was slightly higher in the artificial microbialites (Margalef species richness, 0.771) than

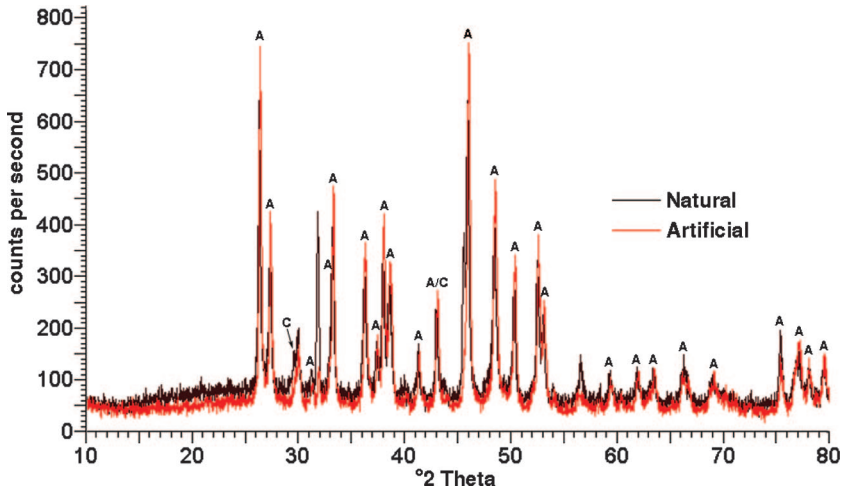

FIG. 2. XRD analyses of biologically precipitated calcium carbonate derived from artificial microbialite and natural stromatolite samples. The calcium carbonate signatures for the artificial microbialite crust layer and natural stromatolites were highly similar and were comprised predominately of the polymorph aragonite (A). Analysis revealed there was slightly less calcite (C) in the artificial samples than in the natural stromatolites.

in the natural stromatolites (Margalef species richness, 0.698). The Shannon index values for the artificial microbialites and natural stromatolites were almost identical. When the diversity indices of the individual layers were compared, the species richness and Shannon index values were lowest for the biofilm layer, whereas the crust layer had the highest diversity of the artificial microbialite layers (Table 2).

Three ARISA bands (at 706, 752, and 899 bp) were chosen for further sequencing analysis based on the pronounced peak areas and presence in the four sample types. The 706-bp band was present only in the artificial microbialite layer samples (biofilm, cyanobacterial, and crust samples). The 752-bp band was present in all samples, whereas the 899-bp band was present only in the cyanobacterial, crust, and natural stromatolite samples. At least five clones of each band for each sample type were sequenced (≥25 clones for each band) and assigned a putative name based on the top BLAST hits for the ITS region's sequences (see Table S1 in the supplemental material).

TABLE 1. Comparison of ARISA profiles of artificial microbialites and natural stromatolites[a]

Peak size (bp)	Biofilm layer		Cyanobacterial layer		Crust layer		Natural stromatolites	
	No. of samples containing peak[b]	Mean peak area	No. of samples containing peak[c]	Mean peak area	No. of samples containing peak[d]	Mean peak area	No. of samples containing peak[d]	Mean peak area
370			4	34.9			2	29.8
397	2	12.8						
465			2	44.1			5	65.9
498			2	18.8				
542							2	36.9
557			1	22.5	2	32.2		
587	1	32.9	8	98.3	8	37.4	6	52.7
616			8	124.4	6	49.2		
634	1	30.5					1	28.4
647			1	16.1	5	50.8	4	44.6
662	6	55.0	5	51.1	5	48.5	6	131.1
682			5	37.7	5	45.7	1	30.2
706[e]	3	24.2	8	443.7	9	119.8		
752[e]	5	92.3	3	238.9	9	211.8	6	101.0
796		-			1	80.1	7	98.4
839	5	119.4	1	98.3	1	311.0	3	129.3
899[e]			8	296.5	9	119.9	7	140.6
982							2	65.6
1,037	1	19.5						
1,171	1	15.0			1	28.2	1	30.3
1,256	1	32.1						

[a] The significant peaks were the peaks for which the values were above the 20-fluorescence unit threshold.
[b] Six different samples were examined.
[c] Eight different samples were examined.
[d] Ten different samples were examined.
[e] Band sizes selected for sequencing and analysis.

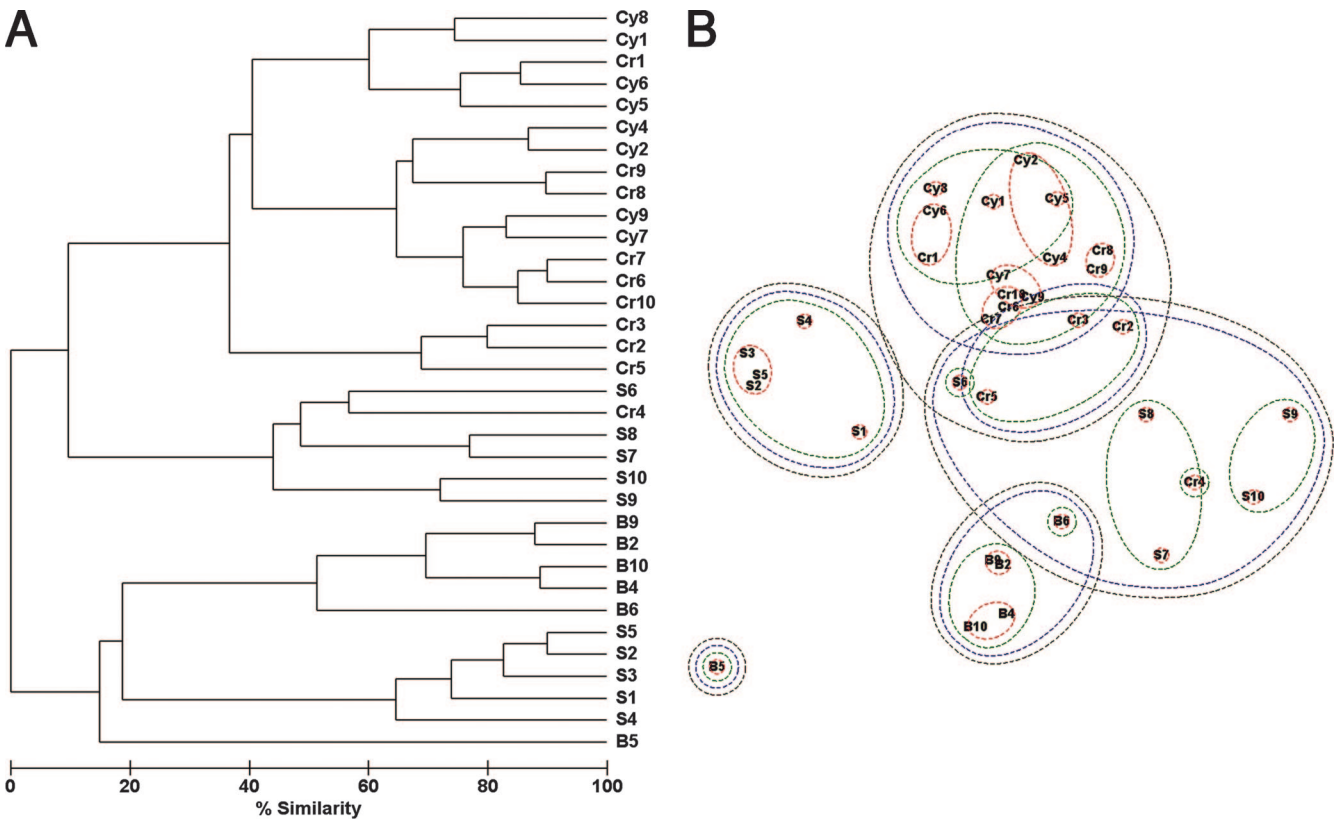

FIG. 3. Cluster analysis of the ARISA profiles for the artificial microbialite and natural stromatolite samples described in Table 1. Abbreviations: B, biofilm layer of the artificial microbialites; Cy, cyanobacterial layer of the artificial microbialites; Cr, crust layer of the artificial microbialites; S, natural stromatolite samples. (A) Phylogenetic tree based on the percent similarity of the ARISA profiles of the samples. (B) Multidimensional scaling plot of the ITS profiles for the artificial microbialite and natural stromatolite samples. The colors of the circles indicate the percentages of similarity for populations (black, 20%; blue, 40%; green, 60%; red, 80%).

The BLAST analyses of most of the ITS regions produced novel results, and the data exhibited less than 90% identity to data in the current ITS database (see Table S1 in the supplemental material). For the artificial microbialites, 32% of the clones recovered from the 706-bp band were similar to the genus *Rhodobacter* (82% sequence identity). The highest levels of similarity to known organisms for the 706-bp clones isolated from the crust layer were the levels of similarity to members of the order *Thiotrichales* (96 to 97%), which are known to be involved in the sulfur cycles in marine sediments (4, 32). In the cyanobacterial layer, the highest levels of similarity to known organisms for the ITS clones were the levels of similarity to the genus *Mesorhizobium* (97%), an uncultured bacterium isolated from a chloroethane superfund site (98%), and the San Pedro Ocean Time series (100%). For the 752-bp band, 45% of the recovered clones were similar to *Sinorhizobium* sp. (80 to 86%). These "*Sinorhizobium*-like" clones were found in all three of the artificial microbialite layers and the natural field-collected stromatolites. Finally, for the 899-bp ITS band, 43% of the clones were similar to the order *Rhizobiales*, but the level of sequence identity was only 77 to 87%. The highest level of sequence similarity for the 899-bp crust and cyanobacterial layer samples was the level of sequence similarity to an uncultured marine bacterium belonging to the San Pedro Ocean Time series (100%), although 10% of the sequenced clones were highly similar (97%) to the alkaliphilic organism *Bacillus halodurans*.

TABLE 2. Univariate diversity indices for ITS regions of artificial microbialites and natural stromatolites

Sample	Margalef species richness	Pielou's evenness value	Shannon index
Biofilm layer	0.598	0.898	1.24
Cyanobacterial layer	0.863	0.793	1.52
Crust layer	0.801	0.868	1.56
Artificial microbialites[a]	0.771	0.851	1.46
Natural stromatolites	0.698	0.931	1.48

[a] The values are cumulative averages for all biofilm, cyanobacterial, and crust samples.

Bacterial diversity of artificial and natural microbialites as determined using 16S rRNA gene analysis. To complement the ARISA community profiles, the bacterial diversity of each artificial microbialite layer was analyzed using 16S rRNA gene analysis and compared to that of the natural field-collected stromatolites (Fig. 4). Most of the major phyla detected in the three artificial microbialite layers were also found in the natural stromatolites. The one exception was the phylum *Verrucomicrobia*, which was detected only in the artificial microbialites. Differences in the major phyla between the three artificial microbialite layers were also observed. In the biofilm layer

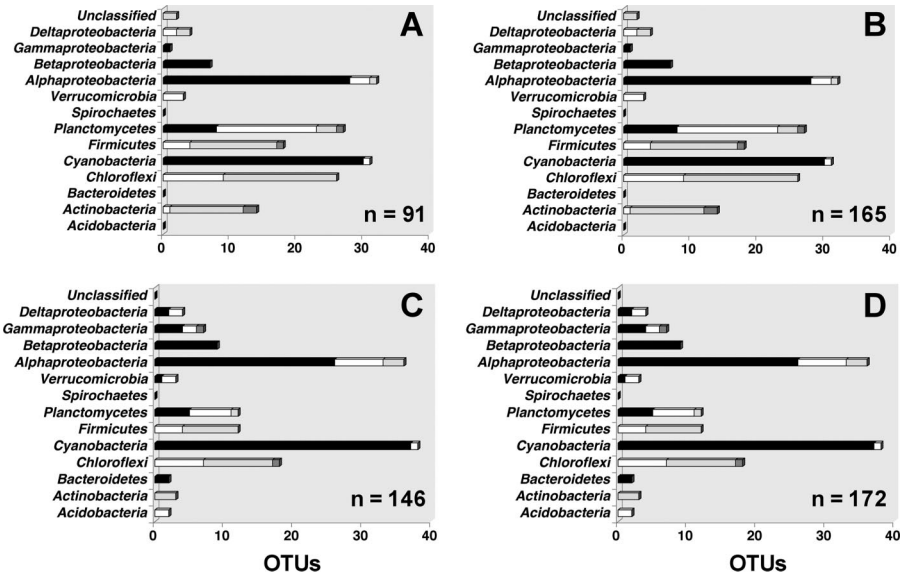

FIG. 4. Diversity of artificial microbialites and natural stromatolites. The graphs show the numbers of OTUs recovered per phylum and the associated DNAML values (black bars, >0.9; open bars, 0.80 to 0.89; light gray bars, 0.7 to 0.79; dark gray bars, < 0.70). The classifications of OTUs are the classifications for (A) the biofilm layer, (B) the cyanobacterial layer, (C) the crust layer, and (D) natural stromatolite samples.

(Fig. 4A), the dominant phylum was the *Proteobacteria*, specifically the class *Alphaproteobacteria* (57%). This class accounted for five times more OTUs (97% identity level) in the biofilm layer than any other class or phylum. Clones with sequence similarity to the *Spirochaetes* were found only in the biofilm layer of the artificial microbialites. The community in the cyanobacterial layer (Fig. 4B) was more diverse than the communities in the other layers, and it included sequences representing the *Alphaproteobacteria* (19%), *Cyanobacteria* (19%), *Planctomycetacia* (16%), *Chloroflexi* (16%), *Firmicutes* (11%), and *Actinobacteria* (8%). In the crust layer (Fig. 4C), the phyla represented were similar to those in the cyanobacterial layer in that the highest numbers of OTUs detected belonged to the phyla *Alphaproteobacteria* (20%) and *Cyanobacteria* (18%). The phyla *Planctomycetes* (8%), *Chloroflexi* (6%), and *Firmicutes* (10%) were also detected in the crust layer.

As in the artificial microbialites, the dominant phyla in the natural stromatolites were the *Alphaproteobacteria* (20%) and *Cyanobacteria* (19%) (Fig. 4D). There were higher numbers of *Delta-*, *Beta-* and *Gammaproteobacteria* (5, 16, and 9%, respectively) in the natural stromatolites than in the artificial microbialites; however, the numbers of members of the phyla *Planctomycetes* (8%), *Chloroflexi* (6%), and *Firmicutes* (10%) were comparable to the numbers in the cyanobacterial and crust layers. Also detected in the natural stromatolites were clones representative of the *Acidobacteria* (0.6%), which were found only in the lithified crust layer of the artificial microbialites. DNA maximum likelihood (DNAML) analysis of the four communities revealed the highest levels of sequence novelty in the *Chloroflexi*, *Planctomycetacia*, *Firmicutes*, and *Actinobacteria*, and the DNAML values were less than 0.89 (Fig. 4). The phyla with the highest DNAML values (>0.90) were the *Alphaproteobacteria* and *Cyanobacteria*.

The 16S rRNA genes recovered from the artificial microbialite layers and natural stromatolites ($n = 582$) were inserted into a bacterial 16S rRNA gene tree containing over 130,000 sequences. The nearest neighbor or isolate for each of the 16S rRNA genes identified in this study was retained in the tree, and all other sequences were removed. The resulting phylogenetic tree (Fig. 5) was consolidated into 66 clusters containing at least two artificial microbialite or natural stromatolite sequences representing 18 different phyla. Many of the recovered 16S rRNA genes were closely related to genes recovered from other microbial mat habitats. For example, clusters 57 to 60 and clusters 62 and 63 contained 98 *Chloroflexi* sequences that were highly similar to sequences found in the microbial mat communities of Guerrero Negro and Lake Vida, Antarctica. The phyla *Bacteroidetes* (cluster 36), *Cyanobacteria* (cluster 42), *Planctomycetes* (clusters 39 and 41), *Proteobacteria* (clusters 10, 13, and 27), and WS6 (cluster 66) also shared sequence similarity with organisms derived from microbial mat habitats (Fig. 5).

Sequence overlap between artificial microbialites and natural stromatolites. The phylogenetic tree also revealed the extent of 16S rRNA sequence similarity between the artificial microbialites and natural stromatolites. The data for each cluster indicate the number of sequences from each of the artificial microbialite layers and natural stromatolites (Fig. 5). More than one-third of the clusters ($n = 25$) contained sequences from both artificial microbialites and natural stromatolites (Fig. 5). One-third of the recovered sequences ($n = 28$) clustered in groups containing only artificial microbialite sequences, and the remaining clusters ($n = 13$) were found only in the natural stromatolites.

The recovered 16S rRNA sequences, however, reflect only a portion of the true bacterial diversity within the microbialite communities. None of the four samples examined in this study were sequenced to community saturation. The percent coverage values revealed that 71% of the artificial microbialite community ecotypes and 60% of the natural stromatolite commu-


Cluster 1 [58 seqs: B=27, Cy=15, Cr=11, S=5]
Rhodopseudomonas julia str. DSM 11549, AY428572.1
Cultivating Sargasso Sea clone GMD21A06, AY162106.1
Strom2E07
Cluster 2 [7 seqs: B=3, Cy=1, Cr=2];
Cultivating Sargasso Sea clone GMD37D2, AY162081.1
Cluster 3 [2 seqs: B=1, Cy=1]
Hypersaline endoevaporitic microbial mat clone E2aE09, DQ103625.1
Cluster 4 [7 seqs: B=1, Cy=4, Cr=2]
Recovery mangrove sediment clone SZB36, AM176847.1
Sinorickettsia chlamys, AY174894.1
CyanoA11
Sagittula stellata, U58356.1
Strom2B08
Citricella thiooxidans str. CHLG 1, AY639887.1
BiofilmG10
Mangrove soil clone MSB-3E12, DQ811852.1
StromA04
Cluster 5 [2 seqs: B=1, S=1]
Maricaulis washingtonensis str. MCS06, AJ227804.1
Cluster 6 [20 seqs: B=5, Cy=2, Cr=5, S=8];
Parvularcula bermudensis str. HTCC2517, AF544016.1
Rhodobacterales
Cluster 7 [3 seqs: B=2, Cr=1]
Cluster 8 [2 seqs: Cr=2];
Brucella sp. str. HJ114, DQ167235.1
Cluster 9 [2 seqs: B=1, Cr=1]
Blastochloris sulfoviridis str. RN1, AB110414.1
Cluster 10 [2 seqs: Cr=1, S=1];
Microbial Mat Black Band-Diseased Siderastrea siderea tissue clone BBD-216_19, DQ446093.1
Roseibium denhamense str. OCh 254, D85832.1
Cyano2D03
Phyllobacterium sp. BBCT68, DQ337552.1
StromA07
Rhizobiales
Cluster 11 [3 seqs: S=3];
Zebrafish digestive tract clone aab5h05, DQ815019.1
Filomicrobium fusiforme str. DSM 5304, Y14313.1
CyanoG12
Municipal wastewater treatment plant clone 054D04_B_DI_P58, CR933225.1
Strom2F01
Cluster 12 [2 seqs: S=2]
Deep-sea octacoral clone ctg_CGOAA69, DQ395471.1
Inactive deep-sea hydrothermal vent chimneys clone IheB2-3, AB099936.1
Strom2D08
Rhodobium gokurnum str. JA 173, AM180706.1
Crust2B07
Bradyrhizobiales
Cluster 13 [2 seqs: S=3];
Microbial Mat Black Band-Diseased Siderastrea siderea tissue clone BBD_217_15, DQ446131.1
Deep-sea sediment clone BD7-3, AB015579.1
Strom2E10
Cluster 14 [2 seqs: B=1, S=1]
Deep-sea octacoral clone ctg_CGOAB08, DQ395494.1
Cluster 15 [3 seqs: Cr=3]
Forest soil clone DUNssu035 (+2C) (OTU#147), AY913254.1
Cluster 16 [3 seqs: Cy=2, Cr=1]
Sponge clone TK34, AJ347030.1
Cluster 17 [3 seqs: Cy=1, Cr=2]
Seawater isolate Rhodospirillaceae str. CL-GR58, EF203900.2
Cluster 18 [7 seqs: B=6, Cr=1]
Sponge clone TK80, AJ347050.1
Mangrove soil clone MSB-2D4, EF125433.1
Strom2D10
Mediterranean Tethya aurantium sponge cortex clone TAA-10-13, AM259857.1
BiofilmG08
Cluster 19 [2 seqs: B=1, S=1];
Symbiont of Oligochaeta from Bermuda and Bahamas clone SpecB-a1-16, AJ890096.1
130m depth HOT station ALOHA 22.45 N 158 deg. W clone HF130_H4_P1, DQ300622.1
Strom2E03
Cluster 20 [2 seqs: Cy=1, Cr=1]
Lake Kauhako 30 m clone K2-30-36, AY344369.1
Inquilinus limosus str. AU430, AY043373.1
Cyano2F06
Terasakiella pusilla str. IFO13613, AB006768.1
Crust2C10
Cluster 21 [2 seqs: B=1, S=1]
Lake Wai'ele'ele water clone LWSR-14, AY345543.1
Alphaproteobacteria
Cluster 22 [3 seqs: B=1, Cr=1, S=1]
Activated 4th maturation stage sludge clone F35-814, EF174262.1
Cluster 23 [47 seqs: B=8, Cy=6, Cr=7, S=26]
Comamonas compostus str. CC-YY287, EF015884.1
Cluster 24 [2 seqs: Cy=1, Cr=1];
Comamonas terrigena str. WAB1888, AM184229.1
Pseudomonas sp. str. JS-1, DQ884343.1
Crust2B05
Betaproteobacteria
Stenotrophomonas sp. str. TR6-01, AB166885.1
StromB05
Cluster 25 [4 seqs: B=1, Cr=1, S=2]
Acinetobacter calcoaceticus str. ATCC 23055T group one, Z93434.1
Cluster 26 [2 seqs: S=2]
Acinetobacter junii str. S33, AB101444.1
Autotrophic nitrifying biofilm clone NB-04, AB117708.1
Strom2G01
Cluster 27 [3 seq: Cy=1, Cr=1, S=1]
Hypersaline endoevaporitic microbial mat clone E2aE11, DQ103665.1
Coxiella burnetii, M21291.1
StromB10
Cecidotrioza sozanica, AF286124.1
Crust2D04
Deep-sea sediment clone NKB5, AB013257.1
StromG12
Cold seep sediment clone JT75-128, AB189370.1
StromA02
Cluster 28 [2 seqs: S=2]
Soil clone X35, DQ083107.1
Cluster 29 [2 seqs: S=2]
Inactive deep-sea hydrothermal vent chimneys clone IndB3-17, AB100006.1
Gammaproteobacteria
Cluster 30 [3 seqs: S=3]
Aspen rhizosphere clone Elev_16S_1371, EF019984.1
Dehalococcoides sp. chlorinated ethene-contaminated aquifer clone W8, DQ223087.1
Strom2G12
Aspen rhizosphere clone Elev_16S_1380, EF019993.1
BiofilmB02
Cluster 31 [2 seqs: B=1, Cy=1];
Surface Marine macro-alga clone UA27, DQ269038.1
Hypersaline microbial mat clone GN01-8.057, DQ154854.1
StromD04
Deep-sea mud volcano clone Amsterdam, BC20-1B-35, AY592339.1
StromF03
Cluster 32 [3 seqs: S=3]
Deep sea sediment clone A144, AY373403.1
South Atlantic Bight Permeable Shelf Sediment clone LC1-13, DQ289938.1
StromB07
Cluster 33 [2 seqs: Cr=2];
Desulfovibrio africanus str. DSM 2603T, X99236.1
Deltaproteobacteria
Cluster 34 [3 seqs: Cy=2, Cr=1]
Cobb Seamount, Juan de Fuca, basalt glass clone JdFBGBact_44, DQ070831.1
Crust2B09
Microbial seeps clone E91-39, DQ001631.1
CyanoH10
Cluster 35 [2 seqs: S=2]
Deep-sea mud volcano clone Amsterdam, BC20-2B-24, AY592384.1
TM6

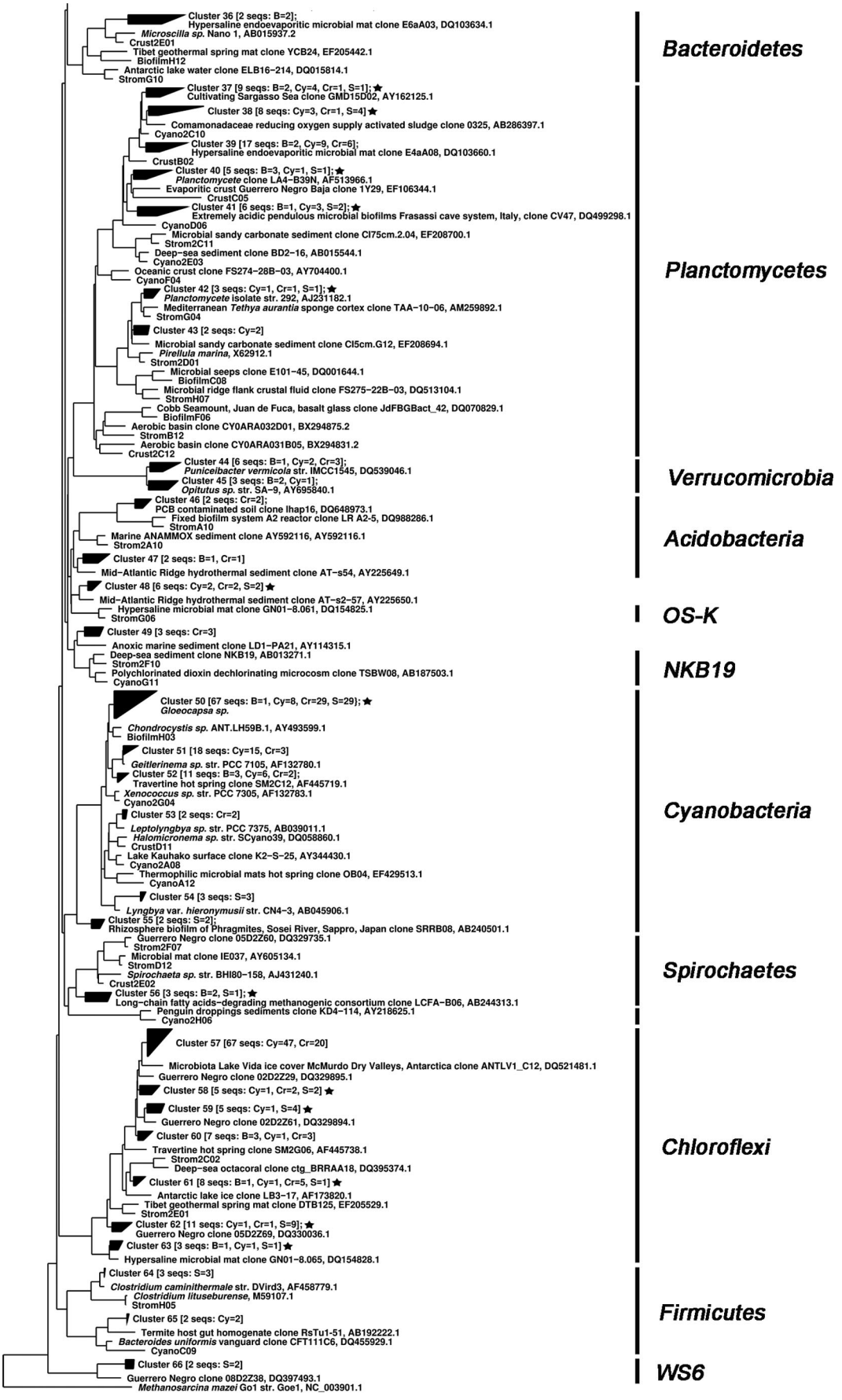
Cluster 36 [2 seqs: B=2];
Hypersaline endoevaporitic microbial mat clone E6aA03, DQ103634.1
Microscilla sp. Nano 1, AB015937.2
Crust2E01
Tibet geothermal spring mat clone YCB24, EF205442.1
BiofilmH12
Antarctic lake water clone ELB16-214, DQ015814.1
StromG10
Bacteroidetes
Cluster 37 [9 seqs: B=2, Cy=4, Cr=1, S=1];
Cultivating Sargasso Sea clone GMD15D02, AY162125.1
Cluster 38 [8 seqs: Cy=3, Cr=1, S=4]
Comamonadaceae reducing oxygen supply activated sludge clone 0325, AB286397.1
Cyano2C10
Cluster 39 [17 seqs: B=2, Cy=9, Cr=6];
Hypersaline endoevaporitic microbial mat clone E4aA08, DQ103660.1
CrustB02
Cluster 40 [5 seqs: B=3, Cy=1, S=1];
Planctomycete clone LA4-B39N, AF513966.1
Evaporitic crust Guerrero Negro Baja clone 1Y29, EF106344.1
CrustC05
Cluster 41 [6 seqs: B=1, Cy=3, S=2];
Extremely acidic pendulous microbial biofilms Frasassi cave system, Italy, clone CV47, DQ499298.1
CyanoD06
Microbial sandy carbonate sediment clone CI75cm.2.04, EF208700.1
Strom2C11
Deep-sea sediment clone BD2-16, AB015544.1
Cyano2E03
Oceanic crust clone FS274-28B-03, AY704400.1
CyanoF04
Cluster 42 [3 seqs: Cy=1, Cr=1, S=1];
Planctomycete isolate str. 292, AJ231182.1
Mediterranean Tethya aurantia sponge cortex clone TAA-10-06, AM259892.1
StromG04
Cluster 43 [2 seqs: Cy=2]
Microbial sandy carbonate sediment clone CI5cm.G12, EF208694.1
Pirellula marina, X62912.1
Strom2D01
Microbial seeps clone E101-45, DQ001644.1
BiofilmC08
Microbial ridge flank crustal fluid clone FS275-22B-03, DQ513104.1
StromH07
Cobb Seamount, Juan de Fuca, basalt glass clone JdFBGBact_42, DQ070829.1
BiofilmF06
Aerobic basin clone CY0ARA032D01, BX294875.2
StromB12
Aerobic basin clone CY0ARA031B05, BX294831.2
Crust2C12
Planctomycetes
Cluster 44 [6 seqs: B=1, Cy=2, Cr=3];
Puniceibacter vermicola str. IMCC1545, DQ539046.1
Cluster 45 [3 seqs: B=2, Cy=1];
Opitutus sp. str. SA-9, AY695840.1
Verrucomicrobia
Cluster 46 [2 seqs: Cr=2];
PCB contaminated soil clone Ihap16, DQ648973.1
Fixed biofilm system A2 reactor clone LR A2-5, DQ988286.1
StromA10
Marine ANAMMOX sediment clone AY592116, AY592116.1
Strom2A10
Cluster 47 [2 seqs: B=1, Cr=1]
Mid-Atlantic Ridge hydrothermal sediment clone AT-s54, AY225649.1
Cluster 48 [6 seqs: Cy=2, Cr=2, S=2]
Mid-Atlantic Ridge hydrothermal sediment clone AT-s2-57, AY225650.1
Hypersaline microbial mat clone GN01-8.061, DQ154825.1
StromG06
Acidobacteria
Cluster 49 [3 seqs: Cr=3]
Anoxic marine sediment clone LD1-PA21, AY114315.1
Deep-sea sediment clone NKB19, AB013271.1
Strom2F10
Polychlorinated dioxin dechlorinating microcosm clone TSBW08, AB187503.1
CyanoG11
OS-K
NKB19
Cluster 50 [67 seqs: B=1, Cy=8, Cr=29, S=29];
Gloeocapsa sp.
Chondrocystis sp. ANT.LH59B.1, AY493599.1
BiofilmH03
Cluster 51 [18 seqs: Cy=15, Cr=3]
Geitlerinema sp. str. PCC 7105, AF132780.1
Cluster 52 [11 seqs: B=3, Cy=6, Cr=2];
Travertine hot spring clone SM2C12, AF445719.1
Xenococcus sp. str. PCC 7305, AF132783.1
Cyano2G04
Cluster 53 [2 seqs: Cr=2]
Leptolyngbya sp. str. PCC 7375, AB039011.1
Halomicronema sp. str. SCyano39, DQ058860.1
CrustD11
Lake Kauhako surface clone K2-S-25, AY344430.1
Cyano2A08
Thermophilic microbial mats hot spring clone OB04, EF429513.1
CyanoA12
Cluster 54 [3 seqs: S=3]
Lyngbya var. hieronymusii str. CN4-3, AB045906.1
Cluster 55 [2 seqs: S=2];
Rhizosphere biofilm of Phragmites, Sosei River, Sappro, Japan clone SRRB08, AB240501.1
Cyanobacteria
Guerrero Negro clone 05D2Z60, DQ329735.1
Strom2F07
Microbial mat clone IE037, AY605134.1
StromD12
Spirochaeta sp. str. BHI80-158, AJ431240.1
Crust2E02
Spirochaetes
Cluster 56 [3 seqs: B=2, S=1];
Long-chain fatty acids-degrading methanogenic consortium clone LCFA-B06, AB244313.1
Penguin droppings sediments clone KD4-114, AY218625.1
Cyano2H06
Cluster 57 [67 seqs: Cy=47, Cr=20]
Microbiota Lake Vida ice cover McMurdo Dry Valleys, Antarctica clone ANTLV1_C12, DQ521481.1
Guerrero Negro clone 02D2Z29, DQ329895.1
Cluster 58 [5 seqs: Cy=1, Cr=2, S=2]
Cluster 59 [5 seqs: Cy=1, S=4]
Guerrero Negro clone 02D2Z61, DQ329894.1
Cluster 60 [7 seqs: B=3, Cy=1, Cr=3]
Travertine hot spring clone SM2G06, AF445738.1
Strom2C02
Deep-sea octacoral clone ctg_BRRAA18, DQ395374.1
Cluster 61 [8 seqs: B=1, Cy=1, Cr=5, S=1]
Antarctic lake ice clone LB3-17, AF173820.1
Tibet geothermal spring mat clone DTB125, EF205529.1
Strom2E01
Cluster 62 [11 seqs: Cy=1, Cr=1, S=9];
Guerrero Negro clone 05D2Z69, DQ330036.1
Cluster 63 [3 seqs: B=1, Cy=1, S=1]
Hypersaline microbial mat clone GN01-8.065, DQ154828.1
Chloroflexi
Cluster 64 [3 seqs: S=3]
Clostridium caminithermale str. DVird3, AF458779.1
Clostridium lituseburense, M59107.1
StromH05
Cluster 65 [2 seqs: Cy=2]
Termite host gut homogenate clone RsTu1-51, AB192222.1
Bacteroides uniformis vanguard clone CFT111C6, DQ455929.1
CyanoC09
Firmicutes
Cluster 66 [2 seqs: S=2]
Guerrero Negro clone 08D2Z38, DQ397493.1
Methanosarcina mazei Go1 str. Goe1, NC_003901.1
WS6
0.10

nity ecotypes were sequenced. For the artificial microbialites, there was 59% coverage for the biofilm, 57% coverage for the cyanobacterial layer, and 59% coverage for the crust layer. Rarefaction curves were based on distance matrices for the 16S rRNA sequences in the forward direction and were determined at the 97% confidence level (data not shown).

The levels of overlap between the natural and artificial systems were comparable to the results obtained in the ITS analysis. Comparison of the ITS and 16S rRNA libraries generated in this study revealed that 47% of all of the nearest neighbors of the ITS sequences were similar to the 16S rRNA nearest neighbors at the family or genus level. At the order level, the level of similarity was 60%; at the class level, 84% of the sequences were comparable; and at the phylum level, 87% of the sequences were similar. In the ITS libraries, there were six unknown *Eubacteria* and six sequences representing two phyla (*Nitrospirae* and *Thermotogae*) that had no counterparts in the 16S rRNA library.

DISCUSSION

The results of this study provide evidence that (i) lithifying microbialite communities can be cultivated under artificial growth conditions, (ii) artificial microbialites precipitate carbonate structures similar to the polymorphs found in natural stromatolites, (iii) natural Bahamian stromatolites harbor a diverse bacterial community dominated by *Proteobacteria* and *Cyanobacteria*, and (iv) artificial microbialites inoculated using natural communities retain much of the natural microbial diversity.

Formation of artificial microbialites. The overall macroscopic and microscopic characteristics of the artificially cultivated microbialites were comparable to those of the natural Bahamian stromatolites. Although morphologically less complex than the natural stromatolite communities, the laboratory-grown communities generated layered microbialites in which there was carbonate deposition. Under our experimental growth conditions, the artificial microbialites had three distinct layers, a biofilm layer, a cyanobacterial layer, and a crust layer. Although lithified laminae were present in this artificial system, we designated the laboratory system a microbialite and not a stromatolite due to the lack of repetitive layering due to carbonate precipitation. The lack of the multiple laminae normally found in the natural stromatolites may have been due to the lack of long-term burial of the microbial mats. The stromatolites of Exuma Sound, Bahamas, are subjected to a high-energy environment in the intertidal and subtidal zones. The turbulent wave action deposits exogenous sand particles for the microbial mat to trap and bind (3). The Bahamian stromatolites can undergo daily, weekly, or annual burial events (17, 50). After these lengthy burial events, the cyanobacteria dominating these stromatolites are able to reactivate photosystem II upon exposure to oxygen and light (33, 43). The eukaryotic algae detected in the surface layers of the stromatolites do not photosynthetically recover from extended burial events as well as the cyanobacteria (43). We suspect that if the artificial system were subjected to repetitive long-term burial events, additional lithified laminae would develop. Despite this caveat, our artificial microbialite model indicates that the carbonate deposition and accretion of the stromatolites are not dependent exclusively on burial of the mats.

The carbonate deposition that occurred in the crust layer of the artificial microbialites was similar to that found in the natural stromatolites. As in the natural system, the predominant polymorph of calcium carbonate in the artificial microbialites was aragonite. Extracellular biomineralization of calcium carbonates cemented the oolitic sand grains several millimeters beneath the microbialite surface. In the natural system, one mechanism by which ooids fuse is through the microboring and micritization of sand grains by cyanobacterial endoliths (39, 49). However, 16S rRNA gene analysis of the artificial microbialites did not identify any clones belonging to the cyanobacterial order *Pleurocapsa* (Fig. 5), which is known to contain endolithic ecotypes. Although bias in PCR amplification or DNA extraction may have precluded detection of *Pleurocapsa* in the artificial microbialites, the results may suggest that additional mechanisms for the formation of extracellular carbonate structures are needed to complement the endolith microboring and micritization that occur in natural stromatolites. The mechanisms for aragonite precipitation do appear to be biogenic, however, as axenic sand grains incubated under similar light/dark and seawater conditions exhibited no biomineralization after 1.5 years.

Natural stromatolite diversity. To compare the changes in microbial diversity in the artificial and natural systems, the natural stromatolites were examined by performing a molecular phylogenetic analysis of the 16S rRNA gene. Eighteen different phyla were detected in the natural samples of type 2 stromatolites, and the *Proteobacteria* (51%) and the *Cyanobacteria* (18%) were the phyla with the highest numbers of recovered sequences. *Firmicutes* (11%), *Planctomycetes* (8%), and *Chloroflexi* (6%) were also detected in the natural community. Several biogeochemical analyses have indicated that five key functional groups are present in the Bahamian stromatolites (6, 20, 58, 59). Sequences recovered from the natural stromatolites corroborate the identification of bacteria known to exhibit the metabolism of these key groups, including photoautotrophs (e.g., clusters 50 to 54), sulfate-reducing bacteria (e.g., cluster 33), sulfide-oxidizing bacteria (e.g., cluster 25), fermentative bacteria (e.g., cluster 64), and aerobic heterotrophs (e.g., cluster 1). These results are comparable to the results for

FIG. 5. Phylogenetic tree of the 582 partial 16S rRNA gene sequences from the artificial and natural microbialite samples. The sequences (length, ~800 bp) were inserted into the Greengenes 16S rRNA gene tree using the ARB software package, and clusters were defined for the artificial and natural microbialite samples (clusters 1 to 66). For each cluster, the number of sequences (seqs) and the sample type (B, biofilm layer of the artificial microbialites; Cy, cyanobacterial layer of the artificial microbialites; Cr, crust layer of the artificial microbialites; S, natural stromatolite samples) are indicated in brackets. Samples located outside a cluster are designated by using the sample type (biofilm [Biofilm], cyanobacterial [Cyano], crust [Crust], or stromatolite [Strom]) and an alphanumeric clone designation. Stars indicate the clusters for which there was overlap between the artificial microbialite and natural stromatolite clone libraries. Scale bar = 0.1 substitution per nucleotide position.

sequences recovered from Shark Bay, Australia, the only other known site where there are accreting marine stromatolites (12, 42), suggesting the possibility that there is a common microbial community structure in modern stromatolites.

Comparison of artificial and natural communities. To compare the overall microbial complexity of the intact natural stromatolites and that of the individual layers of the artificial microbialites, ARISA profiles of the ITS region were used in conjunction with 16S rRNA gene analyses. Although ARISA may underestimate the overall community diversity due to the heterogeneity of the ITS region, coupling ARISA with ribosomal gene clone libraries has proven to be an effective means for comparing different community types and for targeting the spatial organization of specific groups of interest (9, 26, 62). In the artificial microbialites, there was extensive overlap with the natural stromatolite communities after 1.5 years of cultivation. More than one-half of the ARISA peaks ($n = 12$) were conserved in the artificial microbialites and natural stromatolites, whereas only two of the peaks were unique to the natural stromatolites and seven peaks were detected only for the artificial microbialites. The larger number of peaks for the artificial microbialites may reflect the enrichment of microorganisms whose abundance is low in the natural habitat due to environmental conditions, such as high-energy wave action, long-term burial in sand, or the presence of UV radiation, none of which was present in the artificial growth conditions. Such enrichments are not uncommon in artificial microbial mat systems. In cultivated cyanobacterial mats from Antarctica, novel morphotypes and phylotypes were detected in an artificial cyanobacterial mat after 8.5 months of cultivation (54).

ARISA profiling also revealed the extent of community similarity for the natural stromatolites and the three individual artificial microbialite layers. ARISA profiling revealed two distinct natural stromatolite populations; the profile one of these populations exhibited 40% similarity with the profile of the artificial crust layer (Fig. 3B), whereas the other exhibited low sequence similarity (20%) to the artificial biofilm layer. The differences in these two natural populations may reflect a microcommunity of organisms in the stromatolites that was not culturable under laboratory conditions or was not included in the original inoculum used for the artificial microbialites. These results may also reflect the efficiency of vertical cross sectioning of the natural stromatolites.

The three bands in the ARISA profiles (706-, 752-, and 899-bp bands) chosen for sequencing analysis due to their relatively large peak areas and abundance in the artificial and natural microbialites were dominated by *Alphaproteobacteria*, specifically the orders *Rhizobiales* and *Rhodobacteriales*. The sequence similarity to the ITS regions was low for most of the recovered clones, and this may suggest that there are novel organisms in the microbialite community; however, it may also reflect the small size of the Ribosomal Intergenic Spacer Sequence Collection database to which the ITS sequences were compared. Despite this limitation, the prevalence of diazotrophic *Rhizobiales* and *Rhodobacteriales* in the artificial microbialites is consistent with previous analyses of nitrogen fixation in Bahamian stromatolites (53) and in Hamelin Pool of Shark Bay, Australia (42). Previous research has shown that noncyanobacterial nitrogen fixation may be important in mats whose cyanobacterial population tends to contain mostly nonheterocystous cyanobacteria (37, 46, 60, 61), such as cyanobacteria with the sequences recovered in the Highborne Cay stromatolites.

Although the *Alphaproteobacteria* sequences dominated all of the communities examined, clone libraries generated for the 16S rRNA gene revealed spatial differences in the sequences recovered from each of the artificial microbialite layers. The biofilm layer consisted predominately of *Alphaproteobacteria*, but it had the highest number of recovered sequences of purple nonsulfur phototrophs and the only *Spirochaetes* sequence detected in the artificial microbialites. The sequences obtained from the clone libraries generated from the cyanobacterial and crust layers exhibited higher levels of similarity to the sequences obtained from the natural stromatolites, and novel sequences from the phyla *Actinobacteria*, *Chloroflexi*, *Firmicutes*, and *Planctomycetes* were recovered. In the crust layer, most of the recovered sequence diversity was similar to that of the cyanobacterial layer; however, sequences associated with the *Acidobacteria* and the *Gammaproteobacteria* order *Thiotricales* were found only in the crust layer. While these communities were not sequenced to completion, the differences in spatial organization within the artificial microbialites may provide insight into the metabolic processes associated with the development of the natural stromatolite ecosystem. Although *Thiotricales* sequences were recovered only from the crust layer, other sulfide-oxidizing bacteria were found throughout the artificial microbialites (e.g., *Chromatiales*). Previous studies have found biological sulfide oxidation at multiple depths in Highborne Cay stromatolites (58).

Although there have been previous successful attempts to model simulated stromatolite communities in silico (19) and to examine the calcification potential of artificial cyanobacterial mats (34), there have been few examples of microbialites actively formed in culture. The artificial microbialite model developed in this study should provide a unique opportunity to experimentally manipulate communities in vitro and to examine the genetic processes associated with stromatolite accretion and growth. For example, the crust community was the only layer within the artificial microbialites in which there was carbonate deposition. The presence of crust-specific organisms, such as the alkaliphilic organism *B. halodurans*, may provide insight into the microbial communities specific to the biomineralization process. Although this study examined microbialites cultivated for 1.5 years, the observation that distinct layering started at 2 months suggests that the progression of microbialite development can be closely monitored or experimentally manipulated in the lab. Taken together, the results described here indicate that the artificial microbialite model provides a unique experimental platform for future studies of the mechanisms associated with the initiation and development of stromatolite ecosystems.

ACKNOWLEDGMENTS

We thank Stefan Green, Luiz Roesch, and Eric Triplett for their helpful discussions and comments on the manuscript. We also thank

Valentin Craciun of the UF Major Analytical Instrument Center for his assistance with the XRD analysis.

This work was supported by a Florida Space Research and Education grant awarded to J.S.F. by the Florida Space Grant Consortium (UCF Project UCF-0000127787).

REFERENCES

1. **Abed, R. M. M., and F. Garcia-Pichel.** 2001. Long-term compositional changes after transplant in a microbial mat cyanobacterial community revealed using a polyphasic approach. Environ. Microbiol. **3:**53–62.
2. **Altschul, S. F., T. L. Madden, A. A. Schaffer, J. H. Zhang, Z. Zhang, W. Miller, and D. J. Lipman.** 1997. Gapped BLAST and PSI-BLAST: a new generation of protein database search programs. Nucleic Acids Res. **25:** 3389–3402.
3. **Andres, M. S., and R. P. Reid.** 2006. Growth morphologies of modern marine stromatolites: a case study from Highborne Cay, Bahamas. Sediment. Geol. **185:**319–328.
4. **Asami, H., M. Aida, and K. Watanabe.** 2005. Accelerated sulfur cycle in coastal marine sediment beneath areas of intensive shellfish aquaculture. Appl. Environ. Microbiol. **71:**2925–2933.
5. **Awramik, S. A.** 1984. Ancient stromatolites and microbial mats, p. 1–22. *In* Y. Cohen, R. W. Castenholz, and H. O. Halvorson (ed.), Microbial mats: stromatolites, vol. 3. Alan R. Liss, Inc., New York, NY.
6. **Baumgartner, L. K., R. P. Reid, C. Dupraz, A. W. Decho, D. H. Buckley, J. R. Spear, K. M. Przekop, and P. T. Visscher.** 2006. Sulfate reducing bacteria in microbial mats: changing paradigms, new discoveries. Sediment. Geol. **185:** 131–145.
7. **Bebout, B. M., S. P. Carpenter, D. J. Des Marais, M. Discipulo, T. Embaye, F. Garcia-Pichel, T. M. Hoehler, M. Hogan, L. L. Jahnke, R. M. Keller, S. R. Miller, L. E. Prufert-Bebout, C. Raleigh, M. Rothrock, and K. Turk.** 2002. Long-term manipulations of intact microbial mat communities in a greenhouse collaboratory: simulating Earth's present and past field environments. Astrobiology **2:**383–402.
8. **Bray, J. R., and J. T. Curtis.** 1957. An ordination of the upland forest communities of southern Wisconsin. Ecol. Monogr. **27:**326–349.
9. **Brown, M. V., M. S. Schwalbach, I. Hewson, and J. A. Fuhrman.** 2005. Coupling 16S-ITS rDNA clone libraries and automated ribosomal intergenic spacer analysis to show marine microbial diversity: development and application to a time series. Environ. Microbiol. **7:**1466–1479.
10. **Buffan-Dubau, E., O. Pringault, and R. de Wit.** 2001. Artificial cold-adapted microbial mats cultured from Antarctic lake samples. 1. Formation and structure. Aquat. Microb. Ecol. **26:**115–125.
11. **Burne, R. V., and L. S. Moore.** 1987. Microbialites: organosedimentary deposits of benthic microbial communities. Palaios **2:**241–254.
12. **Burns, B. P., F. Goh, M. Allen, and B. A. Neilan.** 2004. Microbial diversity of extant stromatolites in the hypersaline marine environment of Shark Bay, Australia. Environ. Microbiol. **6:**1096–1101.
13. **Cardinale, M., L. Brusetti, P. Quatrini, S. Borin, A. M. Puglia, A. Rizzi, E. Zanardini, C. Sorlini, C. Corselli, and D. Daffonchio.** 2004. Comparison of different primer sets for use in automated ribosomal intergenic spacer analysis of complex bacterial communities. Appl. Environ. Microbiol. **70:**6147–6156.
14. **Cole, J. R., B. Chai, R. J. Farris, Q. Wang, A. S. Kulam-Syed-Mohideen, D. M. McGarrell, A. M. Bandela, E. Cardenas, G. M. Garrity, and J. M. Tiedje.** 2007. The ribosomal database project (RDP-II): introducing myRDP space and quality controlled public data. Nucleic Acids Res. **35:**D169–D172.
15. **de los Rios, A., C. Ascaso, J. Wierzchos, E. Fernandez-Valiente, and A. Quesada.** 2004. Microstructural characterization of cyanobacterial mats from the McMurdo Ice Shelf, Antarctica. Appl. Environ. Microbiol. **70:**569–580.
16. **DeSantis, T. Z., P. Hugenholtz, N. Larsen, M. Rojas, E. L. Brodie, K. Keller, T. Huber, D. Dalevi, P. Hu, and G. L. Andersen.** 2006. Greengenes, a chimera-checked 16S rRNA gene database and workbench compatible with ARB. Appl. Environ. Microbiol. **72:**5069–5072.
17. **Dill, R. F., E. A. Shinn, A. T. Jones, K. Kelly, and R. P. Steinen.** 1986. Giant subtidal stromatolites forming in normal salinity waters. Nature **324:**55–58.
18. **Dravis, J. J.** 1983. Hardened subtidal stromatolites, Bahamas. Science **219:** 385–386.
19. **Dupraz, C., R. Pattisina, and E. P. Verrecchia.** 2006. Translation of energy into morphology: simulation of stromatolite morphospace using a stochastic model. Sediment. Geol. **185:**185–203.
20. **Dupraz, C., and P. T. Visscher.** 2005. Microbial lithification in marine stromatolites and hypersaline mats. Trends Microbiol. **13:**429–438.
21. **Dupraz, C., P. T. Visscher, L. K. Baumgartner, and R. P. Reid.** 2004. Microbe-mineral interactions: early carbonate precipitation in a hypersaline lake (Eleuthera Island, Bahamas). Sedimentology **51:**745–765.
22. **Fenchel, T.** 1998. Artificial cyanobacterial mats: cycling of C, O, and S. Aquat. Microb. Ecol. **14:**253–259.
23. **Fenchel, T.** 1998. Artificial cyanobacterial mats: structure and composition of the biota. Aquat. Microb. Ecol. **14:**241–251.
24. **Fenchel, T.** 1998. Formation of laminated cyanobacterial mats in the absence of benthic fauna. Aquat. Microb. Ecol. **14:**235–240.
25. **Fenchel, T., and M. Kühl.** 2000. Artificial cyanobacterial mats: growth, structure, and vertical zonation patterns. Microb. Ecol. **40:**85–93.
26. **Fisher, M. M., and E. W. Triplett.** 1999. Automated approach for ribosomal intergenic spacer analysis of microbial diversity and its application to freshwater bacterial communities. Appl. Environ. Microbiol. **65:**4630–4636.
27. **Golubic, S., and K. M. Browne.** 1996. *Schizothrix gebeleinii* sp. nova builds subtidal stromatolites, Lee Stocking Island, Bahamas. Arch. Hydrobiol. Suppl. Algol. Stud. **83:**273–290.
28. **Green, S. J., C. Blackford, P. Bucki, L. L. Jahnke, and L. Prufert-Bebout.** 2008. A salinity and sulfate manipulation of hypersaline microbial mats reveals stasis in the cyanobacterial community structure. ISME J. **2:**457–470.
29. **Grotzinger, J. P., and A. H. Knoll.** 1999. Stromatolites in Precambrian carbonates: evolutionary mileposts or environmental dipsticks? Annu. Rev. Earth Planet. Sci. **27:**313–358.
30. **Huber, T., G. Faulkner, and P. Hugenholtz.** 2004. Bellerophon: a program to detect chimeric sequences in multiple sequence alignments. Bioinformatics **20:**2317–2319.
31. **Kalkowsky, E.** 1908. Oolith und stromatolith im Norddeutschen Buntsandstein. Dtsch. Geol. Gesell. Z. **60:**68–125.
32. **Karavaiko, G. I., G. A. Dubinina, and T. F. Kondrat'eva.** 2006. Lithotrophic microorganisms of the oxidative cycles of sulfur and iron. Microbiology **75:**512–545.
33. **Kromkamp, J. C., R. Perkins, N. Dijkman, M. Consalvey, M. Andres, and R. P. Reid.** 2007. Resistance to burial of cyanobacteria in stromatolites. Aquat. Microb. Ecol. **48:**123–130.
34. **Kühl, M., T. Fenchel, and J. Kazmierczak.** 2003. Growth, structure and calcification potential of an artificial cyanobacterial mat, p. 77–102. *In* W. E. Krumbein, D. Paterson, and G. Zavarzin (ed.), Fossil and recent biofilms, a natural history of the impact of life on planet Earth. Kluwer Academic Publishers, Dordrecht, The Netherlands.
35. **Lane, D. J.** 1991. 16S/23S rRNA sequencing, p. 115–175. *In* E. Stackebrant and M. Goodfellow (ed.), Nucleic acid techniques in bacterial systematics. John Wiley & Sons Ltd., New York, NY.
36. **Leuko, S., F. Goh, M. A. Allen, B. P. Burns, M. R. Walter, and B. A. Neilan.** 2007. Analysis of intergenic spacer region length polymorphisms to investigate the halophilic archaeal diversity of stromatolites and microbial mats. Extremophiles **11:**203–210.
37. **Ley, R. E., J. K. Harris, J. Wilcox, J. R. Spear, S. R. Miller, B. M. Bebout, J. A. Maresca, D. A. Bryant, M. L. Sogin, and N. R. Pace.** 2006. Unexpected diversity and complexity of the Guerrero Negro hypersaline microbial mat. Appl. Environ. Microbiol. **72:**3685–3695.
38. **Ludwig, W., O. Strunk, R. Westram, L. Richter, H. Meier, Yadhukumar, A. Buchner, T. Lai, S. Steppi, G. Jobb, W. Forster, I. Brettske, S. Gerber, A. W. Ginhart, O. Gross, S. Grumann, S. Hermann, R. Jost, A. Konig, T. Liss, R. Lussmann, M. May, B. Nonhoff, B. Reichel, R. Strehlow, A. Stamatakis, N. Stuckmann, A. Vilbig, M. Lenke, T. Ludwig, A. Bode, and K. H. Schleifer.** 2004. ARB: a software environment for sequence data. Nucleic Acids Res. **32:**1363–1371.
39. **Macintyre, I. G., L. Prufert-Bebout, and R. P. Reid.** 2000. The role of endolithic cyanobacteria in the formation of lithified laminae in Bahamian stromatolites. Sedimentology **47:**915–921.
40. **Paerl, H. W., and J. L. Pinckney.** 1996. A mini-review of microbial consortia: their roles in aquatic production and biogeochemical cycling. Microb. Ecol. **31:**225–247.
41. **Paerl, H. W., T. F. Steppe, and R. P. Reid.** 2001. Bacterially mediated precipitation in marine stromatolites. Environ. Microbiol. **3:**123–130.
42. **Papineau, D., J. J. Walker, S. J. Mojzsis, and N. R. Pace.** 2005. Composition and structure of microbial communities from stromatolites of Hamelin Pool in Shark Bay, Western Australia. Appl. Environ. Microbiol. **71:**4822–4832.
43. **Perkins, R. G., J. C. Kromkamp, and R. P. Reid.** 2007. Importance of light and oxygen for photochemical reactivation in photosynthetic stromatolite communities after natural sand burial. Mar. Ecol. Prog. Ser. **349:**23–32.
44. **Petrisor, A. I., and A. W. Decho.** 2004. Using geographical information techniques to quantify the spatial structure of endolithic boring processes within sediment grains of marine stromatolites. J. Microbiol. Methods **56:** 173–180.
45. **Petrisor, A. I., T. Kawaguchi, and A. W. Decho.** 2004. Quantifying $CaCO_3$ microprecipitates within developing surface mats of marine stromatolites using GIS and digital image analysis. Geomicrobiol. J. **21:**491–496.
46. **Pinckney, J. L., and H. W. Paerl.** 1997. Anoxygenic photosynthesis and nitrogen fixation by a microbial mat community in a Bahamian hypersaline lagoon. Appl. Environ. Microbiol. **63:**420–426.
47. **Ranjard, L., F. Poly, J. C. Lata, C. Mougel, J. Thioulouse, and S. Nazaret.** 2001. Characterization of bacterial and fungal soil communities by automated ribosomal intergenic spacer analysis fingerprints: biological and methodological variability. Appl. Environ. Microbiol. **67:**4479–4487.
48. **Reid, R. P., I. G. Macintyre, K. M. Browne, R. S. Steneck, and T. Miller.** 1995. Modern marine stromatolites in the Exuma Cays, Bahamas: uncommonly common. Facies **33:**1–17.
49. **Reid, R. P., P. T. Visscher, A. W. Decho, J. F. Stolz, B. M. Bebout, C. Dupraz,**

I. G. Macintyre, H. W. Paerl, J. L. Pinckney, L. Prufert-Bebout, T. F. Steppe, and D. J. DesMarais. 2000. The role of microbes in accretion, lamination and early lithification of modern marine stromatolites. Nature **406:**989–992.
50. **Riding, R., S. M. Awramik, B. M. Winsborough, K. M. Griffin, and R. F. Dill.** 1991. Bahamian giant stromatolites—microbial composition of surface mats. Geol. Mag. **128:**227–234.
51. **Schloss, P. D., and J. Handelsman.** 2005. Introducing DOTUR, a computer program for defining operational taxonomic units and estimating species richness. Appl. Environ. Microbiol. **71:**1501–1506.
52. **Stal, L. J.** 2000. Cyanobacterial mats and stromatolites, p. 61–120. *In* B. A. Whitton and M. Potts (ed.), The ecology of cyanobacteria: their diversity in time and space. Kluver Academic Publishers, Dordrecht, The Netherlands.
53. **Steppe, T. F., J. L. Pinckney, J. Dyble, and H. W. Paerl.** 2001. Diazotrophy in modern marine Bahamian stromatolites. Microb. Ecol. **41:**36–44.
54. **Taton, A., S. Grubisic, E. Brambilla, R. De Wit, and A. Wilmotte.** 2003. Cyanobacterial diversity in natural and artificial microbial mats of Lake Fryxell (McMurdo dry valleys, Antarctica): a morphological and molecular approach. Appl. Environ. Microbiol. **69:**5157–5169.
55. **Tillett, D., and B. A. Neilan.** 2000. Xanthogenate nucleic acid isolation from cultured and environmental cyanobacteria. J. Phycol. **36:**251–258.
56. **Vangemerden, H.** 1993. Microbial mats—a joint venture. Mar. Geol. **113:**3–25.
57. **Visscher, P. T., L. K. Baumgartner, D. H. Buckley, D. R. Rogers, M. E. Hogan, C. D. Raleigh, K. A. Turk, and D. J. Des Marais.** 2003. Dimethyl sulphide and methanethiol formation in microbial mats: potential pathways for biogenic signatures. Environ. Microbiol. **5:**296–308.
58. **Visscher, P. T., R. P. Reid, B. M. Bebout, S. E. Hoeft, I. G. Macintyre, and J. A. Thompson.** 1998. Formation of lithified micritic laminae in modern marine stromatolites (Bahamas): the role of sulfur cycling. Am. Miner. **83:**1482–1493.
59. **Visscher, P. T., and J. F. Stolz.** 2005. Microbial mats as bioreactors: populations, processes, and products. Paleogeogr. Paleoclimatol. Paleoecol. **219:** 87–100.
60. **Yannarell, A. C., and H. W. Paerl.** 2007. Effects of salinity and light on organic carbon and nitrogen uptake in a hypersaline microbial mat. FEMS Microbiol. Ecol. **62:**345–353.
61. **Yannarell, A. C., T. F. Steppe, and H. W. Paerl.** 2006. Genetic variance in the composition of two functional groups (diazotrophs and cyanobacteria) from a hypersaline microbial mat. Appl. Environ. Microbiol. **72:**1207–1217.
62. **Yannarell, A. C., and E. W. Triplett.** 2004. Within- and between-lake variability in the composition of bacterioplankton communities: investigations using multiple spatial scales. Appl. Environ. Microbiol. **70:**214–223.